PAPER

Check for updates

Novel hybrids of thiazolidinedione-1,3,4-oxadiazole derivatives: synthesis, molecular docking, MD simulations, ADMET study, *in vitro*, and *in vivo* anti-diabetic assessment†

Mahendra Gowdru Srinivasa,[a] Jagdish Gopal Paithankar,[b] Sumit Rao Saheb Birangal,[c] Aravinda Pai,[c] Vasudev Pai,[d] Shridhar N. Deshpande[a] and B. C. Revanasiddappa ⓘ *[a]

As compared to standard medicinal compounds, hybrid molecules that contain multiple biologically active functional groups have greater affinity and efficiency. Hence based on this concept, we predicted that a combination of thiazolidinediones and 1,3,4-oxadiazoles may enhance α-amylase and α-glucosidase inhibition activity. A series of novel 3-((5-phenyl-1,3,4-oxadiazol-2-yl)methyl)thiazolidine-2,5-dione derivatives (**5a–5j**) were synthesized and characterized using different spectroscopic techniques *i.e.*, FTIR, ^{1}H-NMR, ^{13}C-NMR and MS. To evaluate *in silico*, molecular docking, MMGBSA, and MD simulations were carried out which were further evaluated *via in vitro* inhibition of α-amylase and α-glycosidase enzyme inhibition assays. In addition, the *in vivo* study was performed on a genetic model of *Drosophila melanogaster* to assess the antihyperglycemic effects. The compounds (**5a–5j**) demonstrated α-amylase and α-glucosidase inhibitory activity in the range of IC$_{50}$ values 18.42 ± 0.21–55.43 ± 0.66 μM and 17.21 ± 0.22–51.28 ± 0.88 μM respectively when compared to standard acarbose. Based on the *in vitro* studies, compounds **5a**, **5b**, and **5j** were found to be potent against both enzymes. *In vivo* studies have shown that compounds **5a**, **5b**, and **5j** lower glucose levels in Drosophila. These compounds could be further developed in the future to produce a new class of antidiabetic agents.

Introduction

Diabetes mellitus (DM) is a chronic metabolic disorder that affects a large number of people.[1] In developed countries, the prevalence of diabetes is likely to rise by 20% among adults and 69% in developing countries by 2030.[2] Glycation of body proteins occurs during diabetes, which results in secondary complications for vital organs. By maintaining ideal blood glucose levels, this process can be inhibited or lowered. Diabetes is treated with insulin and various oral anti-diabetic medications, such as sulphonylureas (*e.g.*, glibenclamide), glinides (*e.g.*, repaglinide), and biguanides (*e.g.*, metformin),

[a]Department of Pharmaceutical Chemistry, NGSM Institute of Pharmaceutical Sciences (NGSMIPS), Nitte (Deemed to Be University), Mangalore-575018, Karnataka, India. E-mail: revan@nitte.edu.in

[b]Division of Environmental Health and Toxicology, Nitte University Centre for Science Education and Research (NUCSER), Nitte (Deemed to Be University), Mangalore-575018, Karnataka, India

[c]Department of Pharmaceutical Chemistry, Manipal College of Pharmaceutical Sciences, Manipal Academy of Higher Education (MAHE), Manipal-5761042, Karnataka, India

[d]Department of Pharmacognosy, Manipal College of Pharmaceutical Sciences, Manipal Academy of Higher Education (MAHE), Manipal-5761042, Karnataka, India

† Electronic supplementary information (ESI) available. See DOI: https://doi.org/10.1039/d2ra07247e

thiazolidinediones (*e.g.*, pioglitazone), and α-amylase, α-glycosidase inhibitors like acarbose, voglibose, miglitol, *etc.* Each class of anti-diabetic drugs exerts its effect differently.[3] There are also some adverse effects such as hypoglycemia, lactic acidosis, liver trouble, and diarrhea caused by these drugs, and they fail to significantly improve diabetic complications. A new class of compounds must be developed, that are more effective with fewer side effects to overcome these problems.[4] As part of the present study, digestive enzymes α-amylase and α-glucosidase were selected as the best targets for the treatment.[5,6] The α-amylase hydrolyzes polysaccharides, such as starch, into glucose and maltose[7] followed by intestinal α-glucosidase enzymes to absorb it into our body.[8] The blood glucose level is modulated by α-amylase inhibitors after a meal. Hence, potential inhibitors of an α-amylase enzyme could be used as chemotherapeutic agents to treat diabetes,[9] additionally, the use of multiple approaches, to diabetes treatment can include α-glucosidase enzyme inhibitors.[10] Because these inhibitors block the enzyme, digestion is slowed; this results in slow glucose absorption. Clinically, acarbose and miglitol both lower postprandial blood glucose levels in the body by inhibiting α-glucosidase. The current type-2 diabetes treatment is acarbose, a tetrasaccharide mimic that inhibits the enzymes α-amylase and α-glucosidase.[11] Moreover, α-amylase and α-glucosidase
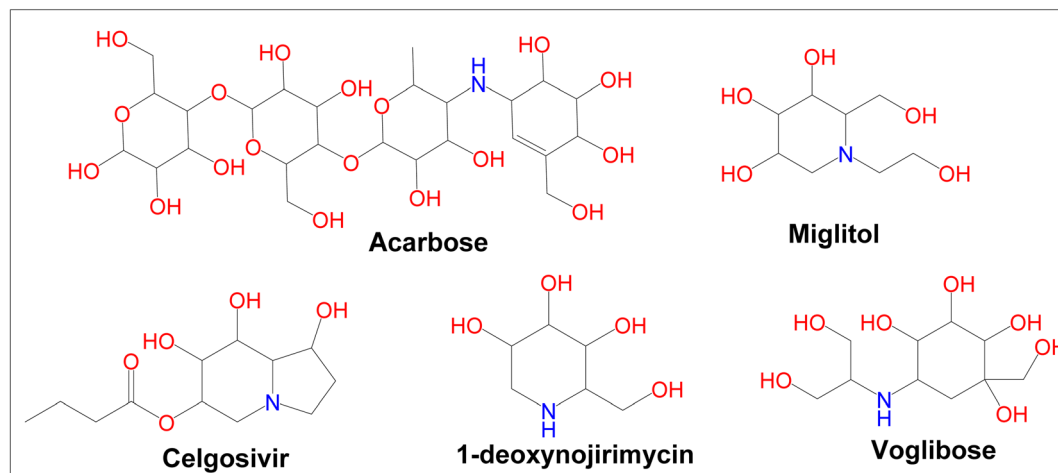
Fig. 1 Currently available α-glucosidase and α-amylase inhibitors.

inhibitors have been found to possess a very large range of biological activities in contrary to antidiabetic drugs such as acarbose, miglitol, celgosivir, 1-deoxynojirimycin, and voglibose (Fig. 1). For example, celgosivir displays antiviral activity against hepatitis C & B viruses, and 1-deoxynojirimycin exhibits anti-cancer activity.[12]

The biological significance of α-amylase and α-glucosidase, along with the inefficiency of currently available drugs make the development of novel inhibitors interesting and challenging.[13] Medicinal chemists are particularly interested in heterocyclic compounds because of their chemical and biological versatility. Therefore, we explored the potential pharmacological effects of heterocyclic organic molecules of various classes and categories as part of our research activity. Thiazolidinedione (TZD) is an attractive pharmacophore to medicinal chemists and pharmaceutical chemists. TZD and its derivatives have a wide range of pharmacological activities, including anti-alzheimer,[14] anti-bacterial,[15] anti-fungal,[16] antiviral,[17] anti-cancer,[18] immunosuppressive,[19] antidiabetic[20] *etc.*

In addition to being an important drug discovery strategy, 1,3,4-oxadiazoles, have a significant impact on numerous findings, such as anti-diabetic,[21] anti-obesity,[22] and anti-cancer.[23] In light of the therapeutic importance of TZD and 1,3,4-oxadiazole moieties, the present study describes the synthesis of a new class of heterocyclic molecules in which both of the molecules are present, as well as an attempt, was made to develop potential bioactive counterparts. The design process involves the use of a new concept. In this study, two active pharmacophores are coupled to create a new structure that exhibits greater activity than any of the previously used pharmacophores. To enhance its potency, we have clubbed thiazolidinedione with 1,3,4-oxadiazole rings with CH_2-linker. The addition of methylene linker increases biological activity. The biochemical actions of these newly synthesized molecules were evaluated for their role in mediating inhibition of α-amylase and α-glucosidase activities using the *in silico*, *in vitro* and *in vivo* studies and also by MD simulation study.

Experimental

Chemistry

Reagents and chemicals were purchased from Sigma Aldrich, Himedia, and SD Fine Chemicals, Mumbai India. Thin-layer chromatography (TLC) was used to examine the homogeneity of the compounds using *n*-hexane and ethyl acetate as a solvent system (2 : 3). The spots were visualized in the UV chamber using pre-coated silica GF_{254} plates. Equiptronics digital melting point apparatus was used for determining the melting points, and the results are uncorrected. FT-IR spectrum (cm^{-1}) was recorded with an Alpha Bruker IR spectrometer. ^{1}H-NMR spectra were recorded using JeolECZ 400 FT-NMR spectrometer operating at 400 MHz and ^{13}C-NMR spectra were recorded using JeolECZ 400 FT-NMR spectrometer operating at 100 MHz. Trimethylsilyl (TMS) was used (δ ppm) as an internal standard. Mass spectra were recorded using the Shimadzu LC-MS-8030 series.

Synthesis of 1,3-thiazolidine-2,4-dione (1)

Chloroacetic acid (0.6 mmol) was dissolved in 6 mL of distilled water and thiourea (0.6 mmol) was dissolved in 6 mL of distilled water and was mixed. The reaction mixture was stirred for 15 minutes at 400 rpm. A white precipitate appeared on cooling in an ice bath. The mixture was heated with stirring (400 rpm) for 10 hours, after adding 6 mL of concentrated hydrochloric acid. The precipitated white compound was filtered, washed, and recrystallized with alcohol.[24]

Synthesis of the potassium salt of 1,3-thiazolidine-2,4-dione (2)

A solution of 1,3-thiazolidine-2,4-dione (1) (0.157 mmol) in ethanol (3.0 mL) was mixed with a solution of potassium hydroxide (0.173 mmol) in ethanol (2.3 mL). An ice bath was used to cool the mixture after stirring (300 rpm) for 2 hours. The crystalline solid was filtered, washed with ethanol, dried, and recrystallized from alcohol.[24]

Synthesis of ethyl 2,4-dioxo-1,3-thiazolidin-3-yl acetate (3)

The potassium salt of 1,3-thiazolidine-2,4-dione (2) (0.066 mmol) was dissolved in dimethylformamide (30 mL) and slowly, ethyl chloroacetate (0.066 M, 7.06 mL) was added. The reaction mixture was refluxed by stirring at 400 rpm for 10 hours. After pouring the mixture into 200 mL of ice-cold water, a reddish-orange liquid gets separated. This was added to 20 mL chloroform, washed with distilled water (three times), and desiccated in anhydrous sodium sulphate. The residual oil was distilled out from the solvent which was extracted under low pressure.

Synthesis of 2-2,4-dioxo-1,3-thiazolidin-3-yl acetohydrazide (4)

The ethyl 2,4-dioxo-1,3-thiazolidin-3-yl acetate (3) was added to absolute ethanol (10 mL), followed by the addition of hydrazine hydrate (0.082 mmol, 99% w/w, 4 mL). The mixture was refluxed for 6 hours and cooled to room temperature. The precipitate was filtered, dried, and re-crystallized using ethanol. (Light brown solid) MP: 192–194 °C; IR (KBr) ν_{max}: cm^{-1}; ^{1}H-NMR (400 MHz, DMSO): (ppm): 9.25 (s, NH, 1H), 4.47 (s, CH$_2$, 2H), 4.23 (s, NH$_2$, 2H), 4.14 (s, CH$_2$, 2H); ^{13}C NMR (DMSO-d$_6$, 100 MHz) δ (ppm); 171.0, 168.6, 162.4, 52.4, and 34.6. LC-MS (m/z): calculated for C$_5$H$_8$N$_3$O$_3$S is 189.1; found: 189.1 (M+).

Synthesis of 3,5-phenyl-1,3,4-oxadiazol-2-yl-methyl thiazolidine-2,5-dione (5a–5j)

To 1 mmol acetohydrazide (4) (5 mL phosphorous oxychloride) with 1 mmol of aromatic acids (4) were added and the mixture was refluxed for about 12–16 hours. After cooling to room temperature, it was poured into crushed ice and the precipitated compound was filtered and neutralized with 20% NaHCO$_3$ the resulting solid mass was filtered, washed with water, and recrystallized in alcohol.[25]

3-((5-(2,4-Dichlorophenyl)-1,3,4-oxadiazol-2-yl)methyl) thiazolidine-2,4-dione (5a). Molecular formula: C$_{12}$H$_7$Cl$_2$N$_3$O$_3$S, yellow solid, yield: 78%, melting point: 210–212 °C; FT-IR (cm^{-1}): 3020 (Ar, C–H), 2927 (CH$_2$), 1734 (C=O), 1585 (C=N), 1513 (C=C). ^{1}H-NMR (400 MHz, DMSO-d$_6$, δ, ppm): 8.78–7.10 (m, Ar–H, 3H), 4.33 (s, CH$_2$, 2H), 3.26 (s, CH$_2$, 2H): ^{13}CNMR (100 MHz, DMSO-d$_6$, δ, ppm): 165.3, 164.2, 163.4, 162.2, 135.0, 129.2, 128.6, 123.3, 122.6, 119.7, 46.3, and 39.0: LC-MS (m/z): calculated for C$_{12}$H$_7$Cl$_2$N$_3$O$_3$S is 344.1; found: 344.1 (M+).

3-((5-(4-Bromophenyl)-1,3,4-oxadiazol-2-yl)methyl) thiazolidine-2,4-dione (5b). Molecular formula: C$_{12}$H$_8$BrN$_3$O$_3$S, yellow solid, yield: 87%, melting point: 185–187 °C; FT-IR (cm^{-1}): 3003 (Ar, CH), 2924 (CH$_2$), 1735 (C=O), 1586 (C=N), 1516 (C=C), 742 (C–Br). ^{1}H-NMR (400 MHz, DMSO-d$_6$, δ, ppm): 7.69–7.11 (m, Ar–H, 4H), 4.41 (s, CH$_2$, 2H), 3.36 (s, CH$_2$, 2H): ^{13}CNMR (100 MHz, DMSO-d$_6$, δ, ppm): 165.9, 159.9, 156.9, 149.8, 129.3, 128.7, 128.6, 123.9, 123.4, 119.7, 45.8, and 34.5: LC-MS (m/z) calculated for C$_{12}$H$_8$BrN$_3$O$_3$S is 354.1; found: 354.1 (M+).

3-((5-(4-Aminophenyl)-1,3,4-oxadiazol-2-yl)methyl) thiazolidine-2,4-dioneone (5c). Molecular formula: C$_{12}$H$_{10}$N$_4$O$_3$S, yellow solid, yield: 82%, melting point: 198–200 °C; FT-IR (cm^{-1}): 3336 (–NH), 3007 (Ar, CH), 2932 (CH$_2$), 1712 (C=O), 1591 (C=N), 1512 (C=C). ^{1}H-NMR (400 MHz, DMSO-d$_6$, δ, ppm): 8.78–8.14 (m, Ar–H, 4H), 7.10 (s, NH$_2$, 2H), 4.98 (s, CH$_2$, 2H), 3.36 (s, CH$_2$, 2H): ^{13}CNMR (100 MHz, DMSO-d$_6$, δ, ppm): 166.0, 164.6, 163.3, 161.2, 144.8, 135.0, 129.2, 128.6, 123.3, 119.4, 45.4, and 33.6: LC-MS (m/z): calculated for C$_{12}$H$_{10}$N$_4$O$_3$S is 290.2; found: 290.2 (M+).

3-((5-(4-Hydroxyphenyl)-1,3,4-oxadiazol-2-yl)methyl) thiazolidine-2,4-dione (5d). Molecular formula: C$_{12}$H$_9$N$_3$O$_4$S, yellow solid, yield: 73%, melting point: 192–194 °C; FT-IR (cm^{-1}): 3315 (–OH), 3020 (Ar, C–H), 2927 (CH$_2$), 1734 (C=O), 1585 (C=N), 1513 (C=C). ^{1}H-NMR (400 MHz, DMSO-d$_6$, δ, ppm): 9.41 (s, OH, 1H), 8.19–7.11 (m, Ar–H, 4H), 4.54 (s, CH$_2$, 2H), 3.35 (s, CH$_2$, 2H): ^{13}CNMR (100 MHz, DMSO-d$_6$, δ, ppm): 165.4, 164.6, 163.4, 161.7, 149.8, 135.0, 129.3, 128.6, 123.4, 119.7, 45.4, and 34.6: LC-MS (m/z): calculated for C$_{12}$H$_9$N$_3$O$_4$S is 291.2; found: 291.2 (M+).

3-((5-Phenyl-1,3,4-oxadiazol-2-yl)methyl)thiazolidine-2,4-dione (5e). Molecular formula: C$_{12}$H$_9$N$_3$O$_3$S, yellow solid, yield: 69%, melting point: 215–217 °C; FT-IR (cm^{-1}): 3017 (Ar, CH), 2857 (CH$_2$), 1736 (C=O), 1598 (C=N), 1515 (C=C). ^{1}H-NMR (400 MHz, DMSO-d$_6$, δ, ppm): 8.40–7.11 (m, Ar–H, 5H), 3.35 (s, CH$_2$, 2H), 3.05 (s, CH$_2$, 2H): ^{13}CNMR (100 MHz, DMSO-d$_6$, δ, ppm): 167.0, 165.7, 163.2, 162.1, 131.5, 129.3, 128.6, 124.4, 123.3, 119.7, 45.8, and 35.2: LC-MS (m/z): calculated for C$_{12}$H$_9$N$_3$O$_3$S is 275.2; found: 275.2 (M+).

3-((5-(4-Methoxyphenyl)-1,3,4-oxadiazol-2-yl)methyl) thiazolidine-2,4-dione (5f). Molecular formula: C$_{13}$H$_{11}$N$_3$O$_4$S, yellow solid, yield: 86%, melting point: 178–180 °C; FT-IR (cm^{-1}): 3046 (Ar, CH), 2896 (CH$_2$), 1687 (C=O), 1584 (C=N), 1515 (C=C). ^{1}H-NMR (400 MHz, DMSO-d$_6$, δ, ppm): 8.16–7.07 (m, Ar–H, 4H), 4.34 (s, CH$_2$, 2H), 3.83 (s, OCH$_3$, 3H), 3.32 (s, CH$_2$, 2H): ^{13}CNMR (100 MHz, DMSO-d$_6$, δ, ppm): 168.8, 166.2, 165.1, 163.0, 161.8, 128.5, 124.0, 123.3, 119.7, 53.4, 45.4, and 33.6: LC-MS (m/z): calculated for C$_{13}$H$_{11}$N$_3$O$_4$S is 305.3; found: 305.3 (M+).

3-((5-(4-Chlorophenyl)-1,3,4-oxadiazol-2-yl)methyl) thiazolidine-2,4-dione (5g). Molecular formula: C$_{12}$H$_8$ClN$_3$O$_3$S, yellow solid, yield: 81%, melting point: 172–174 °C; FT-IR (cm^{-1}): 3035 (Ar, CH), 2920 (CH$_2$), 1731 (C=O), 1592 (C=N), 1517 (C=C). ^{1}H-NMR (400 MHz, DMSO-d$_6$, δ, ppm): 8.16–7.09 (m, Ar–H, 4H), 3.89 (s, CH$_2$, 2H), 3.38 (s, CH$_2$, 2H): ^{13}CNMR (100 MHz, DMSO-d$_6$, δ, ppm): 167.9, 164.7, 162.2, 161.7, 142.3, 135.0, 129.2, 128.6, 123.3, 119.7, 46.7, and 34.4: LC-MS (m/z): calculated for C$_{12}$H$_8$ClN$_3$O$_3$S is 309.7; found: 309.3 (M+).

3-((5-(2-Chloro-4-nitrophenyl)-1,3,4-oxadiazol-2-yl)methyl) thiazolidine-2,4-dione (5h). Molecular formula: C$_{12}$H$_7$ClN$_4$O$_5$S, yellow solid, yield: 74%, melting point: 161–163 °C; FT-IR (cm^{-1}): 3046 (Ar, CH), 2924 (CH$_2$), 1734 (C=O), 1585 (C=N), 1514 (C=C). ^{1}H-NMR (400 MHz, DMSO-d$_6$, δ, ppm): 8.19–7.11 (m, Ar–H, 3H), 4.14 (s, CH$_2$, 2H), 3.36 (s, CH$_2$, 2H): ^{13}CNMR (100 MHz, DMSO-d$_6$, δ, ppm): 165.9, 164.3, 161.9, 161.0, 149.8, 135.0, 129.3, 128.6, 123.4, 119.7, 44.8, and 34.5: LC-MS (m/z): calculated for C$_{12}$H$_7$ClN$_4$O$_5$S is 354.7; found: 354.7 (M+).

3-((5-(4-Nitrophenyl)-1,3,4-oxadiazol-2-yl)methyl) thiazolidine-2,4-dione (5i). Molecular formula: C$_{12}$H$_8$N$_4$O$_5$S, yellow solid, yield: 81%, melting point: 153–155 °C; FT-IR (cm^{-1}): 3005 (Ar, CH), 2955 (CH$_2$), 1735 (C=O), 1582 (C=N),

1514 (C=C). ^{1}H-NMR (400 MHz, DMSO-d$_6$, δ, ppm): 8.12–7.69 (m, Ar–H, 4H), 3.83 (s, CH$_2$, 2H), 3.02 (s, CH$_2$, 2H): ^{13}CNMR (100 MHz, DMSO-d$_6$, δ, ppm): 164.9, 164.0, 163.2, 162.1, 149.2, 135.105, 129.3, 128.6, 123.4, 119.7, 44.7, and 34.4: LC-MS (m/z): calculated for $C_{12}H_8N_4O_5S$ is 320.2795; found: 320.2735 (M+).

3-((5-(2,4-Dihydroxyphenyl)-1,3,4-oxadiazol-2-yl)methyl) thiazolidine-2,4-dione (5j). Molecular formula: $C_{12}H_9N_3O_5S$, yellow solid, yield: 73%, melting point: 204–206 °C; FT-IR (cm^{-1}): 3326 (–OH), 3005 (Ar, CH), 2955 (CH$_2$), 1769 (C=O), 1591 (C=N), 1521 (C=C). ^{1}H-NMR (400 MHz, DMSO-d$_6$, δ, ppm): 10.14 (s, OH, 2H), 7.92–7.09 (m, Ar–H, 4H), 4.43 (s, CH$_2$, 2H), 3.32 (s, CH$_2$, 2H): ^{13}CNMR (100 MHz, DMSO-d$_6$, δ, ppm): 165.5, 164.6, 161.4, 149.3, 135.1, 130.4, 128.3, 122.9, 119.6, 45.4, and 34.5: LC-MS (m/z): calculated for $C_{12}H_9N_3O_5S$ is 307.2; found: 307.2 (M+).

In silico analysis

Docking studies. The docking study was performed using the Glide module from Schrodinger 2020-3 suite Maestro (https://www.schrodinger.com) device installed on a Linux workstation.

Ligand preparation. Chemdraw database (http://www.cambridgesoft.com) was used to obtain the designed compounds, which were arranged using the Schrodinger suite's LigPrep module (https://www.schrodinger.com). To ensure consistent biological activity, the high-energy ionization and tautomers were excluded during the production process with the Epik tool. We simulated the ligands before using virtual screening, to identify and separate the ligands that did not obey Lipinski's rules by using the Qikprop module (https://www.schrodinger.com/products/qikprop).

Preparation of protein. The protein was prepared using the preparation wizard tool. The structure of the glucoamylase enzyme in 3D form was obtained from the RCSB Protein Data Bank (https://www.rcsb.org). The PDB ID: 3TOP shows glucoamylase at a resolution of 2.3 Å treated by adding missing hydrogen, assigning regular bonding format, treating for metal; removing molecules of water which lie 5 Å apart from their heterogeneous groups. The bonds of hydrogen were optimized using sample orientation. All polar group hydrogen was displayed and the structure of the protein was finally minimized to its default root mean square deviation value of 0.30 Å.[26]

Protein–ligand docking. The receptor grid denotes the region of the target protein, where the ligand sampling was performed during the process of molecular docking. It was established using the receptor grid generation interface in the Glide tool of Maestro. It was performed using the force field of OPLS-2005. Using LigPrep defined receptor folders from the grid were selected and docking was made flexible with the extra precision (XP) option on the Glide module. These bindings were ranked on computerized scores consisting of the grid score, Glide score (proprietary), and energy strain (internal). The results were viewed on the pose-viewer in the form of structural output formats. For predicting the binding affinity and ligand ranking, the Glide score was used. The molecular docking study was conducted on the extra precision (XP) mode of the docking program of α-amylase and α-glucosidase inhibitors.

Molecular mechanics/generalized Born surface area (MM/GBSA) assay. The Glide docking was performed in XP mode without applying any constraints. A local optimization feature minimizes the docked poses (Prime v4.9). The MM-GBSA continuum solvent model computes the binding free energies of the docked complexes. This incorporates the OPLS3 force field, a VSGB 2.0 implicit solvent model, and the rotamer search algorithms.[27]

Molecular dynamics (MD) simulation studies. Molecular dynamics simulations were performed using the Schrödinger LLC package (https://www.schrodinger.com/products/desmond)[28] and the studies were carried out for 100 ns on compound **5j** based on Glide dock XP scores using the Maestro 12.6 Desmond panel. 1000 frames were produced and intervals of 20 ps were reported during these simulation studies. To gain a better understanding of ligand–protein interactions and their binding affinities, dynamic experiments were used. Under orthorhombic boundary conditions, systems for the 3TOP–**5j** complexes were designed using a predefined SPC solvation model. The buffering approach was used to measure the box size. To neutralize the charges on the models, sodium and chloride ions were used. The designed systems were subjected to energy minimization using 2000 iterations and a convergence threshold of 25 kcal mol^{-1} Å^{-1}. NPT ensemble class simulations of the minimized complexes were carried out at a 300 K temperature and 1 bar pressure.[29]

Evaluation of ADME-toxicity of compounds (5a–5j). The ADMET properties of all the new compounds were predicted by using the Qikprop module, to find out the drug-like properties. QikProp module version 5.4 of Maestro, Schrodinger (https://www.schrodinger.com/products/qikprop) was used to calculate the molecular descriptor and to predict the ADME profile of these compounds.

Drug-likeness prediction. The OSIRIS property explorer (https://www.organic-chemistry.org/prog/peo) generally uses chemical structures and then calculates various drug-relevant properties on valid structures. The resulting predictions are given values and color codes. The TPSA, log S calculation, c log P calculation, molecular weight, drug score, fragment based drug-likeness, and toxicity are some of the properties analyzed.[30]

Biological activity

In vitro **α-amylase inhibitory assay.** The reaction mixture contains 20 μL of α-amylase solution (0.5 mg mL^{-1}) and 200 μL of sodium phosphate buffer (pH 6.9, 0.02 M). Test samples (10–50 g mL^{-1}) were added (250 μL) to the reaction mixture following which; incubation was carried out for 10 min at room temperature. This was accompanied by the addition of 200 μL of 1% starch solution, and further incubated for 10 min at 25 °C. By adding 400 μL of dinitrosalicylic acid (DNS) reagent, the reaction was terminated. Lastly, it was incubated in water (70 °C, 5 min). The absorbance was recorded using an ELISA microplate reader at 540 nm. As a standard, acarbose was used. All the experiments were performed in triplicates. It was the

reaction mixture without the test sample that served as the control for the test.[31]

The percent inhibition was calculated as:

$$\% \text{ Inhibition} = [(C - T)/C] \times 100$$

C – absorbance of control, T – absorbance of sample.

In vitro α-glycosidase inhibitory assay. The reaction mixture contains 50 μL of 0.1 M phosphate buffer (pH = 6.8), 10 μL of α-glucosidase enzyme and 20 μL of test samples (10–50 μg mL^{-1}) were taken in a 96-well plate and incubated at 37 °C for 15 min. Furthermore, 20 μL of p-nitrophenyl D-glucopyranoside solution was added as a substrate and incubated for an additional 20 min at 37 °C. 50 μL of 0.1 M Na$_2$CO$_3$ is added to terminate the reaction. The liberated p-nitrophenol was measured at 405 nm with an Elisa microplate reader. Acarbose served as the standard and control was set up in parallel without the test substance. All the experiments were performed in triplicates.[31]

The inhibition was calculated in percentage as:

$$\% \text{ Inhibition} = [(C - T)/C] \times 100$$

C – absorbance of control, T – absorbance of sample.

Drosophila culture and experimental design. In this study, Oregon-R flies were obtained directly from the Nitte University, Drosophila Lab, Mangalore, India, and maintained on a wheat cream-agar medium with a relative humidity of 65–70%, and a light–dark cycle of twelve hours each. Separation of males and females of one-day-old flies were cultured in, food containing high sugar diet (HSD), and different groups of food containing HSD with uniform concentrations (18 μg g^{-1} feed) of the compounds **5a, 5b, 5j** for 10 days. Acarbose was administered as a positive control. Twenty flies were taken and they were homogenized in 0.2 mL of ice-cold phosphate buffer saline. (pH 7.4). Homogenized samples were centrifuged at 10 000g for 15 min at 4 °C. All fly homogenates were tested for glucose concentration using the manufacturer's protocol (Agape Diagnostics Ltd, India). Throughout the experiments, the control group was maintained in the same conditions as that of other groups except for HSD and compounds. All experiments were carried out in triplicates and the results were expressed in percentages respective to the control group.[32]

Data analysis. The results of all the experiments ($n = 3$) were analyzed and expressed as mean ± standard deviation (SD). The Student's t-test was performed using GraphPad Prism software (GraphPad Software Inc., CA, USA). p values ≤ 0.05 were considered as statistically significant (*p ≤ 0.05; *p ≤ 0.01; **p ≤ 0.001).

MTT assay. The cytotoxic concentration of synthetic compounds (**5a–5j**) was evaluated by MTT assay. A standard MTT assay was performed with various concentrations of synthesized compounds against NIH/3T3 cells using a 96-well microplate reader at 570 nm. The cell lines were cultured in DMEM, supplemented with 10% FBS in flasks, and incubated at 37 °C with 5% CO$_2$ in DMEM medium with streptomycin and penicillin (100 IU mL^{-1}) at the appropriate concentrations. The 96-well plates with media were incubated. After overnight incubation, each plate was discarded and fresh medium was added to each well with varying concentrations (5 μM, 10 μM, 25 μM, 50 μM, 100 μM) of test samples. Then, 200 μL of MTT (0.5 mg mL^{-1}) were put in each well and further incubated for four hours. Afterward, DMSO (100 μL) was transferred into each microplate well. The absorbance was measured at 570 nm to determine how much MTT was reduced to formazan in the cells. The IC$_{50}$ value was recorded for the samples causing 50% cytotoxicity for all of the cell lines.[33]

Results and discussion

The synthesis of the titled compounds (**5a–5j**) has been represented in Fig. 2. All the new compounds and intermediates were purified by successive recrystallization from ethanol. The purity of the compound was confirmed through melting points and TLC using silica gel G plates as stationary phase and n-hexane and ethyl acetate as a solvent system (2 : 3). Table 1 lists the physicochemical features of the final synthesized compounds. Based on spectral data, FT-IR, ^{1}H NMR, ^{13}C-NMR, and LCMS, the possible structures of all the compounds were established.

The IR spectra of compound **5a** depicted the absorption bands at 3020 for aromatic (C–H), 2927 (CH$_2$), and 1611 (C=N), respectively. The presence of C=O absorption bands was observed at 1734 cm^{-1}, the key functional group in the thiazolidinedione ring. In the ^{1}H-NMR spectra of the compound, **5a** revealed the singlet signal for CH$_2$ at δ 3.26 & 4.33 regions respectively. The aromatic protons were observed as multiplets in the region δ 7.10–8.78. The mass spectrum of compound **5a** showed a molecular ion peak at m/z = 344.17 (M+), which is in agreement with the assigned molecular formula C$_{12}$H$_7$Cl$_2$N$_3$O$_3$S. The ^{13}C-NMR spectra of compound, **5a** showed the presence of required carbon atoms and the presence of key lactone groups.

Docking results

The synthesized compounds bind at the active site of the target PDB: 3TOP (the crystal structure of the α-glucoamylase), in the groove of the target binding site. This might be important in understanding their role as a signal transducer, in diabetes which targets α-glucosidase and α-amylase enzymes. We expressed the binding affinity of these derivatives as G scores (Table 2). The binding free energy of all derivatives ranged from −9.942 to −5.085. In terms of binding energies, compounds **5a**, **5c**, and **5j** have the greatest binding scores, with binding energy values of −6.217, −6.039, and −6.56, respectively (Table 2). Acarbose showed the highest binding affinity towards the target with binding free energies of −9.942. The compound **5j** which was the most active compound in the dataset presents a conventional hydrogen bond with the carbonyl group in the thiazolidinedione ring with *Thr1369* and *Thr1586* residue. The hydroxyl group of the aromatic ring interacted with *Asp1420*, *Arg1510*, and *Asp1526* residue. The aromatic ring and 1,3,4-oxadiazole ring provides pi–pi linkage interaction with *Phe 1559* and *Phe1560* residue. Other amino acid interactions like *Tyr1251*, *Asp1279*, *Ile1315*, *Trp1355*, *Trp1418*, *Met1471*, *Trp1523*, and *Hie1584* showed in Fig. 3.
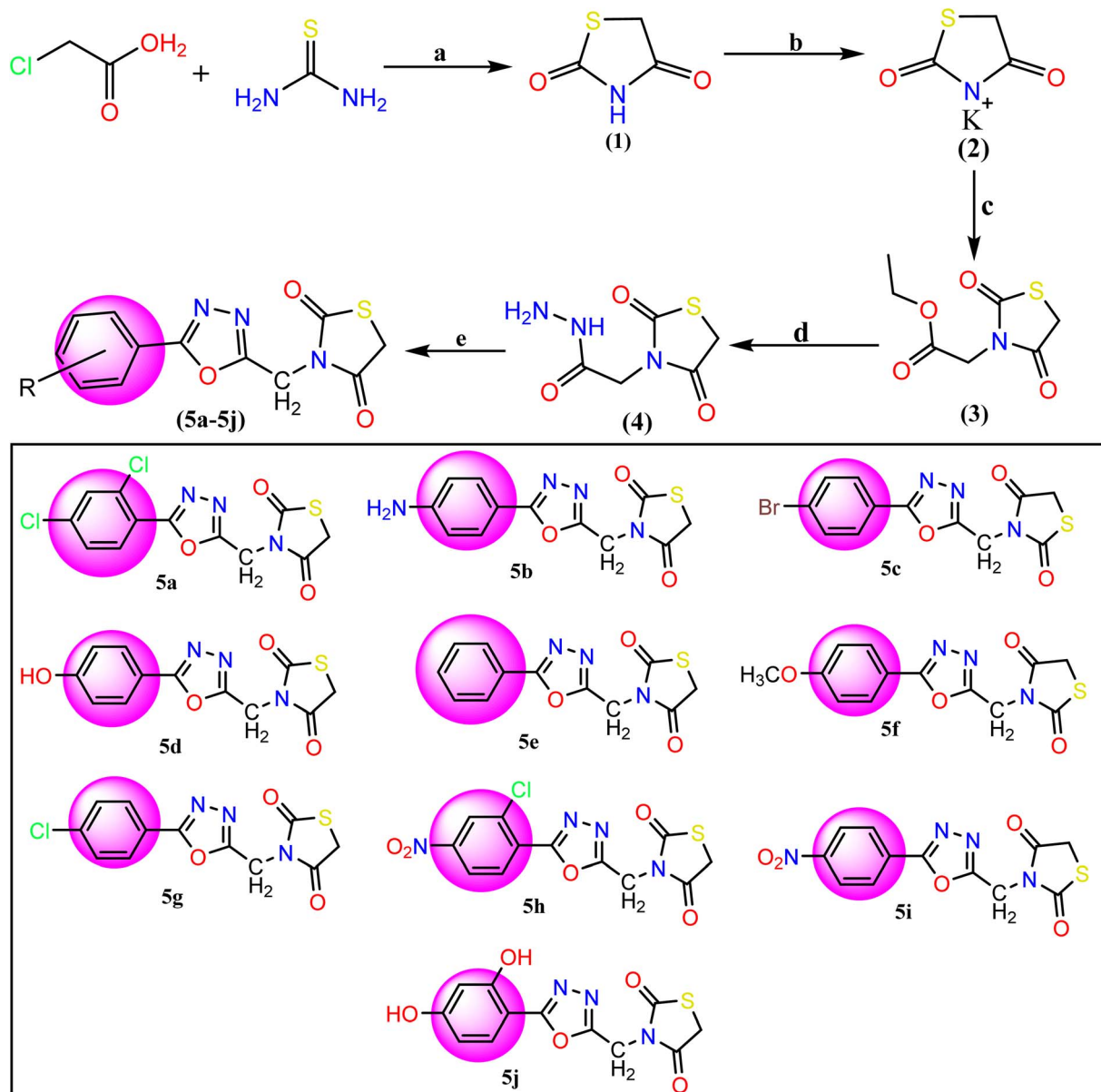
Fig. 2 Reagents and conditions for the synthesis of TZD-1,3,4-oxadiazole derivatives (**5a**–**5j**): (a) dilute HCl and refluxed at 400 rpm for 10 hours with stirring. (b) Ethanolic KOH at room temperature with stirring, (c) ethyl chloroacetate and DMF, (d) hydrazine hydrate and ethanol mixture were refluxed for 6 h. (e) Aromatic acids and POCl$_3$ were added and the mixture was refluxed for about 12–16 h **5a**: 2,4-(Cl)$_2$, **5b**: 4-NH$_2$, **5c**: 4-Br, **5d**: 4-OH, **5e**: C$_6$H$_5$, **5f**: 4-OCH$_3$, **5g**: 4-Cl, **5h**: 2-Cl-4-NO$_2$, **5i**: 4-NO$_2$, **5j**: 2,4-(OH)$_2$.

Compound **5a** showed a hydrogen bond with the carbonyl group in the thiazolidinedione ring with *Hie1584* residue. The chlorine group substituted with the aromatic ring of the halogen bond provides interaction with *Trp1569* residue. The aromatic ring and 1,3,4-oxadiazole ring provides pi–pi linkage interaction with *Trp1355*, *Phe1559*, and *Phe1560* residue. Other amino acid interaction includes *Pro1159*, *Asp1157*, *Tyr1167*, *Tyr1251*, *Asp1279*, *Trp1418*, *Asp1420*, *Met1421*, *Lys1460*, *Arg1510*, *Trp1523*, *Asp1526*, and *Thr1526*. The compound **5b** had a hydrogen bond with the carbonyl group in the thiazolidinedione ring with *Hie1584* residue. The bromine group substituted with an aromatic ring of halogen bond provided interaction with Trp1369 residue (Fig. 3). The 1,3,4-oxadiazole ring showed pi–pi linkage interaction with
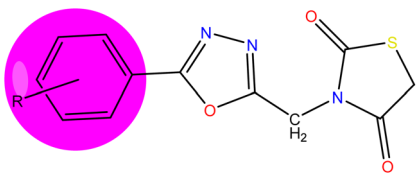
Trp1355 residue. Other amino acid interactions like *Asp1157*, *Pro1159*, *Tyr1251*, *Asp1279*, *Trp1418*, *Asp1420*, *Met1421*, *Lys1460*, *Asp1526*, and *Thr1586*. Based on the docking scores, the selected candidates were found to be good for diabetic activity.

MM/GBSA assay

For the best-ranking molecules, the binding free energy calculations of molecular mechanics/generalized Born surface area (MM/GBSA) were performed. To estimate the relative affinity of ligand binding to the receptor, the Glide XP mode was used. All molecules were with good binding-free energy and their values were observed from −22.39 to −52.32 kcal mol^{-1} (Table 3). To obtain

Table 1 Physicochemical properties of compounds (**5a**–**5j**)

Compounds	R	Molecular formula	Molecular weight	MP (°C)	Yield (%)
5a	2-4-(Cl)$_2$	C$_{12}$H$_7$Cl$_2$N$_3$O$_3$S	344.172	210–212	78
5b	4-Br	C$_{12}$H$_8$BrN$_3$O$_3$S	354.177	185–187	87
5c	4-NH$_2$	C$_{12}$H$_{10}$N$_4$O$_3$S	290.296	198–200	82
5d	4-OH	C$_{12}$H$_9$N$_3$O$_4$S	291.281	192–194	73
5e	C$_6$H$_5$	C$_{12}$H$_9$N$_3$O$_3$S	275.282	215–217	69
5f	4-OCH$_3$	C$_{13}$H$_{11}$N$_3$O$_4$S	305.308	178–180	86
5g	4-Cl	C$_{12}$H$_8$ClN$_3$O$_3$S	309.726	172–174	81
5h	2-Cl-4-NO$_2$	C$_{12}$H$_7$ClN$_4$O$_5$S	354.724	161–163	74
5i	4-NO$_2$	C$_{12}$H$_8$N$_4$O$_5$S	320.279	153–155	81
5j	2,4-(OH)$_2$	C$_{12}$H$_9$N$_3$O$_5$S	307.284	204–206	73

Table 2 Glide docking scores (kcal mol^{-1}) of the compounds (**5a**–**5j**) on enzyme PDB ID: 3TOP

Compounds	Extra-precision docking score (kcal mol^{-1})			
	Gscore[a]	Gemodel[b]	Gecou[c]	evdW[d]
5a	**−6.217**	−61.651	−5.886	−38.494
5b	**−6.039**	−59.164	−5.219	−37.307
5c	−6.037	−57.182	−6.948	−35.563
5d	−5.958	−55.244	−7.573	−35.379
5e	−5.085	−51.949	−2.969	−35.257
5f	−5.885	−55.499	−4.709	−35.959
5g	−5.974	−55.115	−4.937	−35.578
5h	−5.928	−65.157	−6.622	−40.067
5i	−6.026	−57.822	−5.71	−37.578
5j	**−6.56**	−57.559	−13.566	−28.709
Acarbose	−9.942	−87.212	−28.178	−29.573

[a] Glide score. [b] Glideemodel (model energy, emodel). [c] Glideecoul (Coulomb energy). [d] Glide evdw (van der Waals energy).

the ΔG bind calculations, the optimal poses from XP dock complexes **5a**, **5c**, and **5j** were chosen. The reliability of this approach for grading the affinity of the designed molecules binding to their respective target proteins has been reported. The MM-GBSA score produces a significant correlation with the experimentally determined results. The compounds **5a**, **5c**, and **5h** showed −51.06 kcal mol^{-1}, −50.12 kcal mol^{-1}, and −52.32 kcal mol^{-1} respectively which are favorable binding energies. However, in the present case, **5h** has shown the best binding free energy and the results of the same are shown in Table 3.

Molecular dynamics simulation

Among the synthesized molecules, the compound **5j** was further extended for the molecular dynamics simulation study. Based on an explicit hydration environment, a 100 ns MD simulation was performed to assess compound **5j**'s stability in a complex with 3TOP. MD simulation results were analyzed using root-mean-standard deviation (RMSD), root-mean-square fluctuation (RMSF), and protein–ligand contact mapping. An important parameter of the MD simulation trajectory used to predict Cα deviation in a dynamic environment is protein Cα RMSD. The RMSD of **5j** fluctuated in the first phase of the simulation up to 45 ns, then increased to 2.3 Å and equilibrated until the end. A protein's RMSD graph revealed stability from 45 to 100 ns, with an RMSD range of 1.8 to 2.4 Å a good result. Over time, RMSF calculates the average deviation from the initial position for each protein residue. A specific component of the protein structure that deviates from the mean is examined by the RMSF. When protein molecules are bound to a small molecule, the RMSF of each amino acid can be used to determine the stability of the bound protein molecules. When MD simulation is performed, proteins with higher RMSF values indicate greater flexibility, while proteins with lower RMSF values suggest less flexibility. A plot of the RMSF of each amino acid of the 3TOP protein bound to compound **5j** is shown in Fig. 4B. The compound **5j** contacts 37 amino acids of the 3TOP as shown in Fig. 4B. Protein interactions with the ligand were monitored throughout the simulation. In the stipulated duration, Tyr1251, and Trp1369 demonstrated hydrophobic interaction with compound **5j**. Further, hydrogen bond interaction was observed with amino acid residues such as Asp1370 and Asp1420. The MD simulation revealed ionic, amino-acid-mediated hydrogen bond interactions with the compound **5j**, the simulation also revealed hydrophobic interaction. Fig. 4C shows the specific sequence contacts between the various amino acid residues present in the complex **5j**–3TOP.

Absorption, distribution, metabolism, and excretion (ADME) properties of compounds (5a–5j) using QikProp

The QikProp pharmacokinetic parameters provide relevant details such as molecular weight, partition coefficient, oral
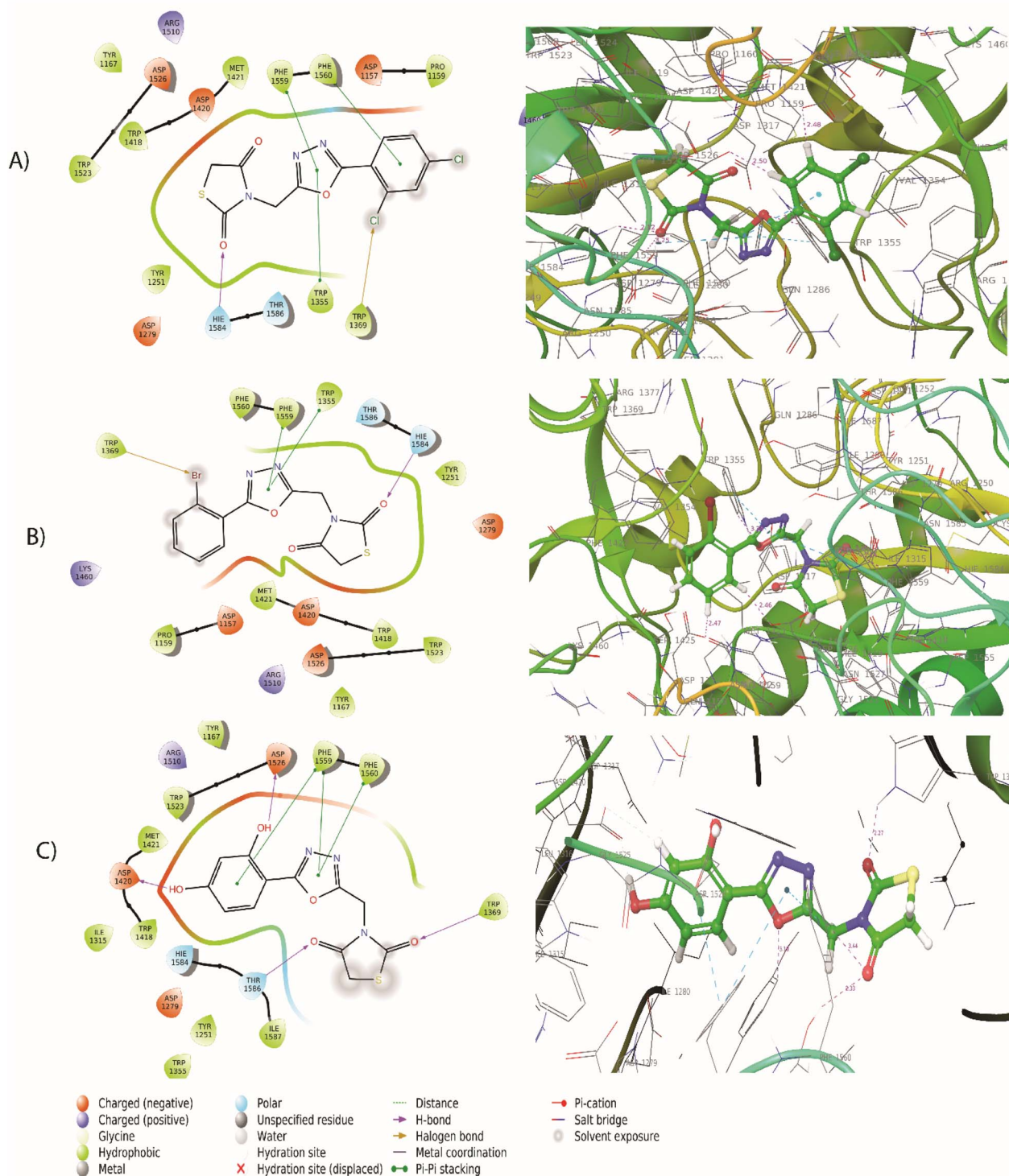
Fig. 3 (A) 2D and 3D interaction of compound **5a** with 3TOP (B) 2D and 3D interaction of compound **5b** with 3TOP (C) 2D and 3D interaction of compound **5j** with 3TOP.

absorption percentage, properties of Lipinski's (rule of five), and Caco2 cellular permeability (in nm s^{-1}). To estimate the absorption and distribution of drugs within the body, the partition coefficient (QP log P_0/w) range from −2.0 to 6.5 for every ten molecules. An important factor governing drug metabolism and access to biological membranes is Caco2 cell permeability (QPPCaco), which is observed between 128.256 and 1470.581. All the synthesized compound's access to the central nervous system (CNS) is determined by the blood/brain coefficients (Q log B/B). Based on the predicted permeability of Madin canine kidney cells (QPPMDCK), studies reported that ligands with a <25 nm s^{-1} value have poor permeability,

Table 3 MM-GBSA approach for compounds (5a–5j)[a]

Compounds	ΔG bind (kcal mol^{-1})	ΔG bind Coulomb	ΔG bind covalent	ΔG bind van der	ΔG bind H bond	ΔG bind lipophilic
5a	−51.06	−13.7	3.23	−42.37	−0.35	−27.15
5b	−50.12	−12.15	2.48	−39.79	−0.39	−24.66
5c	−22.39	−16.23	2.47	−37.11	−4.61	−18.22
5d	−22.79	−15.5	2.56	−38.05	−1.49	−18.59
5e	−23.76	−7.49	1.78	−40.35	−0.13	−22.24
5f	−45.56	−9.54	2.48	−40.26	−0.41	−22.98
5g	−48.45	−10.83	3.11	−39.54	−0.39	−24.69
5h	−52.32	−7.58	3.97	−44.13	−1.08	−24.63
5i	−49.11	−3.29	2.64	−41.83	−0.6	−21.34
5j	−29.21	−18.46	4.58	−32.32	−2.35	−18.33
Acarbose	−46.21	−119.36	18.97	−33.45	−8.32	−43.55

[a] ΔG bind: free energy of binding; ΔG bind Coulomb: Coulomb energy; ΔG bind covalent: covalent energy (internal energy); ΔG bind van der: van der Waals energy; ΔG bind H bond: hydrogen bonding energy; ΔG bind lipophilic: hydrophobic energy (non-polar contribution estimated by solvent accessible surface area).

whereas ligands with a >500 nm s^{-1} value have a great deal of potential to be drug-like molecules. The overall human oral absorption percentage for compounds ranged from 85.8 to 100%. PSA describes a molecule's ability to form hydrogen bonds. In humans, this information correlates with the number of drugs absorbed through the intestinal tract. PSA > 140 Å

indicates poor absorption of a molecule. There are 95% of synthesized compounds with PSA < 140 Å, which indicates that these molecules are well absorbed by the digestive system. All these pharmacokinetic parameters were found within the acceptable range defined for human use except acarbose (standard) as shown in Table 4. Based on this, we analyzed ten

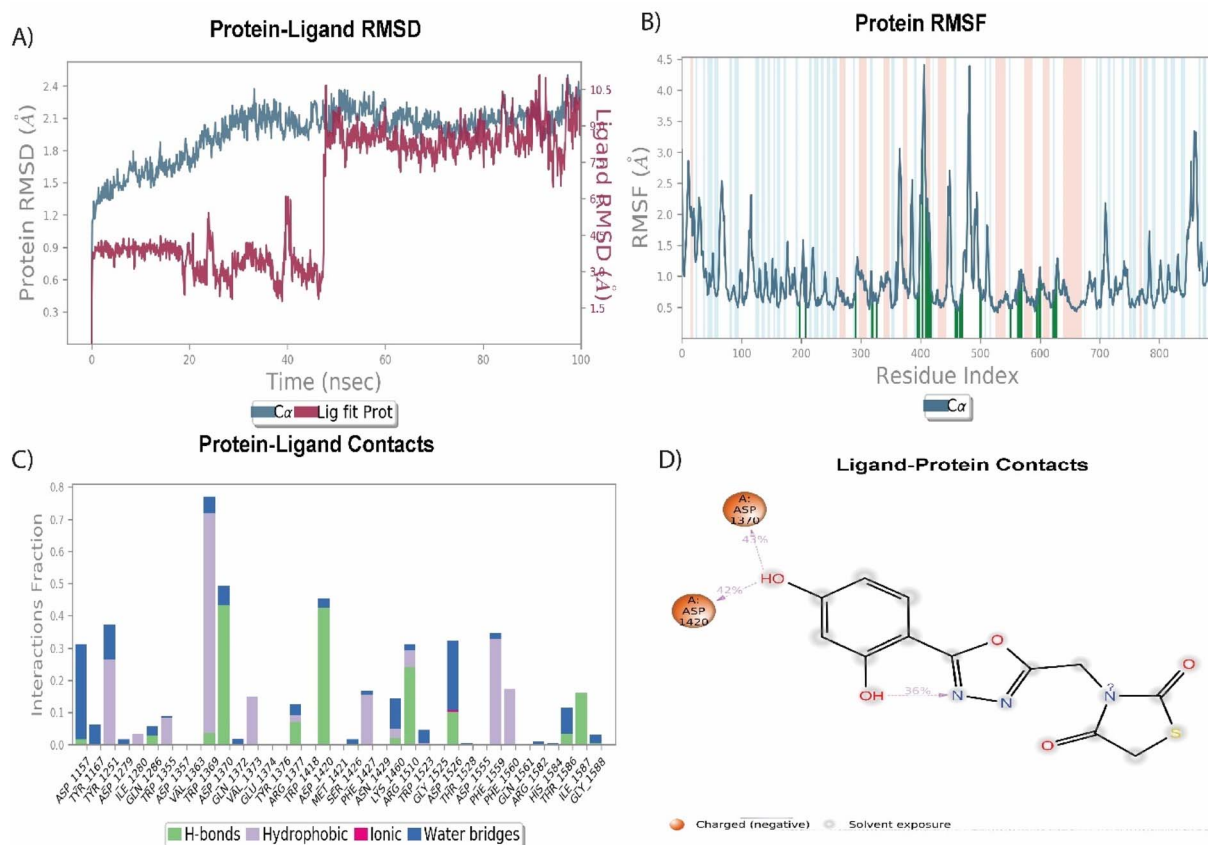**Fig. 4** MD simulation analysis of 5j in complex with enzyme active site (PDB ID: 3TOP) (A) RMSD (protein RMSD is shown in grey while RMSD of compound 5j is shown in red), (B) protein RMSF, (C) protein–ligand contact analysis of MD trajectory and (D) 2D interaction diagram.

Table 4 ADME properties of compounds (**5a–5j**) using QikProp[a]

Comp.	HB donor	HB acceptor	QP log P_0/w	QPPCaco	QP log B/B	QPPMDCK	PHOA	PSA	Rule of five
Acceptable range	≤5	≤10	−2 to 6.5	25 poor; >500 great	−3 to 1.2	<25 poor; >500 great	>80% high; <25% low	≤140	≤5
5a	0	5.5	2.556	631.261	−0.29	2936.205	92.029	95.604	0
5b	0	5.5	2.13	649.365	−0.414	1318.433	89.758	95.386	0
5c	1.5	6.5	1.045	136.105	−1.292	108.943	71.259	124.17	0
5d	1	6.25	1.234	157.879	−1.23	127.894	73.516	120.092	0
5e	0	5.5	1.585	524.643	−0.645	468.378	84.904	97.801	0
5f	0	6.25	1.642	520.906	−0.746	464.759	85.182	105.819	0
5g	0	5.5	2.09	524.617	−0.501	1156.401	87.866	97.786	0
5h	0	6.5	1.461	75.543	−1.456	119.714	69.114	140.611	0
5i	0	6.5	0.616	62.767	−1.66	47.194	64.283	142.671	0
5j	2	6.5	1.245	146.285	−1.430	1186.224	90.156	126.268	0
Acarbose	13	32.1	−7.276	0.04	−5.765	0.01	0	317.259	3

[a] HB donor: hydrogen bond donor; HB acceptor: hydrogen bond acceptor; QPPCaco: predicted apparent Caco-2 cell permeability in nm s^{-1}; QP log B/B: predicted brain/blood partition coefficient; QPPMDCK: predicted apparent MDCK cell permeability; PHOA: percentage of human oral absorption: PSA: predicted polar surface area.

compounds from the most active to the least active molecule as shown in Table 4, indicating that they are possessing drug-like molecules.

Drug-likeness prediction using Osiris property

Based on Osiris property explorer predictions, the results of toxicity risks and drug score assessments for synthesized compounds (**5a–5j**) are shown in Table 5. Using this tool, we can predict compounds based on their functional groups, which are similar to our extensively studied compounds by *in vitro* methods. There are three color codes for the results: red, green, and yellow.[26] In the green color, there is low toxicity, in the yellow color there are mild toxins and in the red color, there is a high probability of toxicity. The results indicate that all the compounds showing green color would be safe and did not show toxicity concerning tumorigenicity, mutagenicity, irritant effect, and effect on the reproductive system. All the synthesized compounds showed drug-like properties for their drug scores, drug-likeness scores, and other biochemical and toxicity

factors. All the synthesized compounds showed an acceptable range of physicochemical and toxicity parameters as shown in Table 5.

In vitro antidiabetic activity

All the newly synthesized compounds (**5a–5j**) were subjected to an *in vitro* antidiabetic assay by using α-amylase and α-glucosidase methods. The testing of the synthesized derivatives was carried out at a concentration range of 10–50 μg mL^{-1}. Acarbose was used as a standard drug. The results are shown in Table 6.

In the α-amylase assay, some of the tested compounds like **5a, 5c, 5h, 5i**, and **5j** showed very potent activity with IC$_{50}$ values of 18.61 ± 0.22 μM, 22.60 ± 0.48 μM, 23.19 ± 0.31 μM, 21.12 ± 0.23 μM, 18.42 ± 0.21 μM respectively, when compared to the standard acarbose with IC$_{50}$ value 24.35 ± 1.44 μM. In general, the compounds with the presence of electron-withdrawing groups are showing the highest potent activity. However, it is also observed that compounds like **5b** (IC$_{50}$ value 34.08 ± 0.48 μM) and **5f** (IC$_{50}$ value 39.23 ± 0.52 μM) also displayed moderate

Table 5 Drug likeness/scores and toxicity calculation of compounds (**5a–5j**) based on Osiris property explorer

Compounds	Drug-relevant properties				Toxicity			
	C log P	Solubility	Drug likeness	Drug score	Tumorigenic	Reproductive effect	Irritant effect	Mutagenicity
5a	1.97	−4.76	4.94	0.91	Green	Green	Green	Green
5b	1.49	−4.13	−0.47	0.63	Green	Green	Green	Green
5c	0.08	−3.37	2.00	0.90	Green	Green	Green	Green
5d	0.42	−3.00	2.05	0.90	Green	Green	Green	Green
5e	0.76	−3.29	3.54	0.95	Green	Green	Green	Green
5f	0.69	−3.31	−0.72	0.63	Green	Green	Green	Green
5g	1.37	−4.03	3.50	0.93	Green	Green	Green	Green
5h	0.45	−4.49	−3.21	0.48	Green	Green	Green	Green
5i	−0.16	−3.75	−8.37	0.47	Green	Green	Green	Green
5j	0.07	−2.70	3.16	0.93	Green	Green	Green	Green
Acarbose	−7.18	0.59	−7.40	0.29	Green	Green	Green	Green

Table 6 *In vitro* antidiabetic activity of compounds (5a–5j)[a]

Compounds	IC$_{50}$ values	
	α-Amylase (μM)	α-Glucosidase (μM)
5a	18.61 ± 0.22	17.58 ± 0.19
5b	22.60 ± 0.34	22.25 ± 0.22
5c	34.08 ± 0.48	27.25 ± 0.23
5d	55.43 ± 0.66	45.28 ± 0.79
5e	32.43 ± 0.46	33.52 ± 0.45
5f	39.23 ± 0.52	51.28 ± 0.83
5g	28.87 ± 0.36	27.25 ± 0.24
5h	23.19 ± 0.31	28.25 ± 0.31
5i	21.12 ± 0.23	25.23 ± 0.28
5j	18.42 ± 0.21	17.21 ± 0.22
Acarbose	24.35 ± 1.44	23.73 ± 1.22

[a] All results expressed are the mean of three individual replicates ($n = 3$, ±SD).

to weak activity, due to the presence of electron-donating groups on the aromatic ring.

In the α-glucosidase assay, the results revealed that the tested compounds like **5a**, **5b**, and **5j** displayed very potent inhibitory activity with IC$_{50}$ values in the range of 17.58 ± 0.19 μM, 22.25 ± 0.22 μM, 17.21 ± 0.22 μM respectively when compared to the standard acarbose with IC$_{50}$ value 23.73 ± 1.22 μM. The presence of electron-withdrawing groups (chloro, bromo) on the aromatic ring is showing the highest potent activity. However, a decrease in the activity was also observed in the compounds like **5d** (IC$_{50}$ value 45.28 ± 0.79 μM) and **5f** (IC$_{50}$ value 51.28 ± 0.83 μM) due to the presence of electron-donating groups (hydroxyl, methoxy). The presence of the phenyl group showed a very moderate activity by the compound **5e** (IC$_{50}$ value 33.52 ± 0.45 μM).

In vivo study

Drosophila flies were treated with three synthesized compounds, namely **5a**, **5b**, and **5j** based on *in vitro* screening for enzyme inhibition and docking analysis.[34] As a positive

control, acarbose was used. According to the glucose estimation in the fly whole-body homogenates, acarbose-supplemented groups had significantly lowered glucose levels in HSD along with acarbose groups. The reduction in glucose level was found to be about 62%. Similar to acarbose, the synthesized compounds also showed a significant reduction in glucose levels of both male and female fly groups fed on HSD with synthesized compounds (**5a**, **5b**, and **5j**).

The percent reduction in glucose levels was found to be 27.7, 28.4, and 29.05% for **5a**, **5b**, and **5j** respectively in male flies. Whereas the reduction in glucose levels was 12.1, 7.03, and 37% for **5a**, **5b**, and **5j** treated female fly groups (Fig. 5). However, at a given concentration, these tested compounds showed less activity, compared to commercially available acarbose. However, this reduction in antihyperglycemic activity was significant for **5b** and **5j** whereas, this activity was insignificant for **5a**. The antihyperglycemic effects of the tested compounds can be improved by increasing their doses.[35,36]

Structure–activity relationship

The detailed SAR of the compounds is summarized in Fig. 6. The SAR study reveals, that combination of two pharmacophores *viz.*, thiazolidinedione and 1,3,4-oxadiazole moiety will enhance the diabetic activity by the incorporation of methylene linker.

MTT assay

The MTT assay was used to measure the effects of synthesized compounds on NIH-3T3 cells as shown in Fig. 7. MTT is a yellow water-soluble tetrazolium dye that is reduced by live cells to a purple formazan product, insoluble in aqueous solutions. The amount of formazan generated is directly proportional to the number of viable cells. The synthesized compounds during 24 h of incubation induced 87.4–0% inhibition of cellular viability in comparison to the control. In this study, the highest concentration (100 μmol) was used to calculate percentage inhibition.
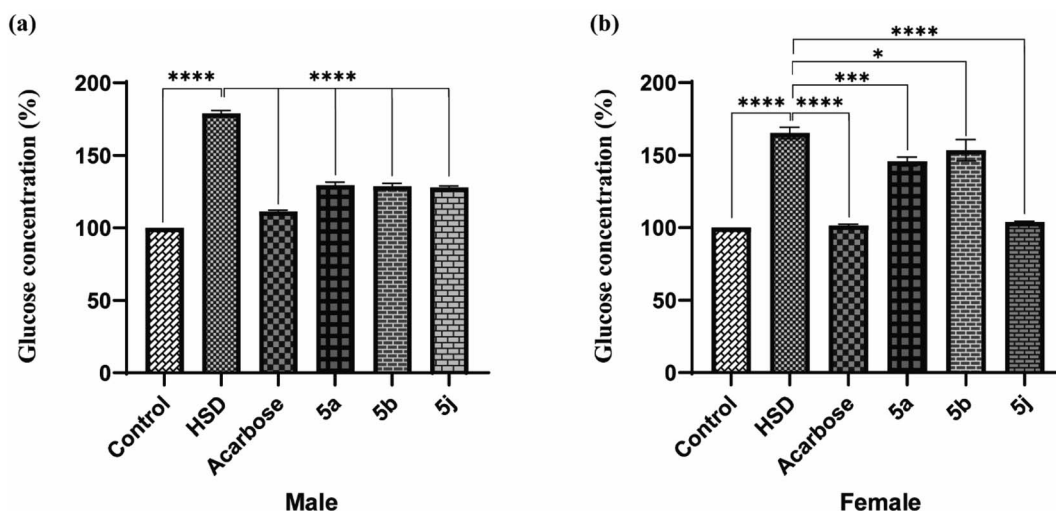

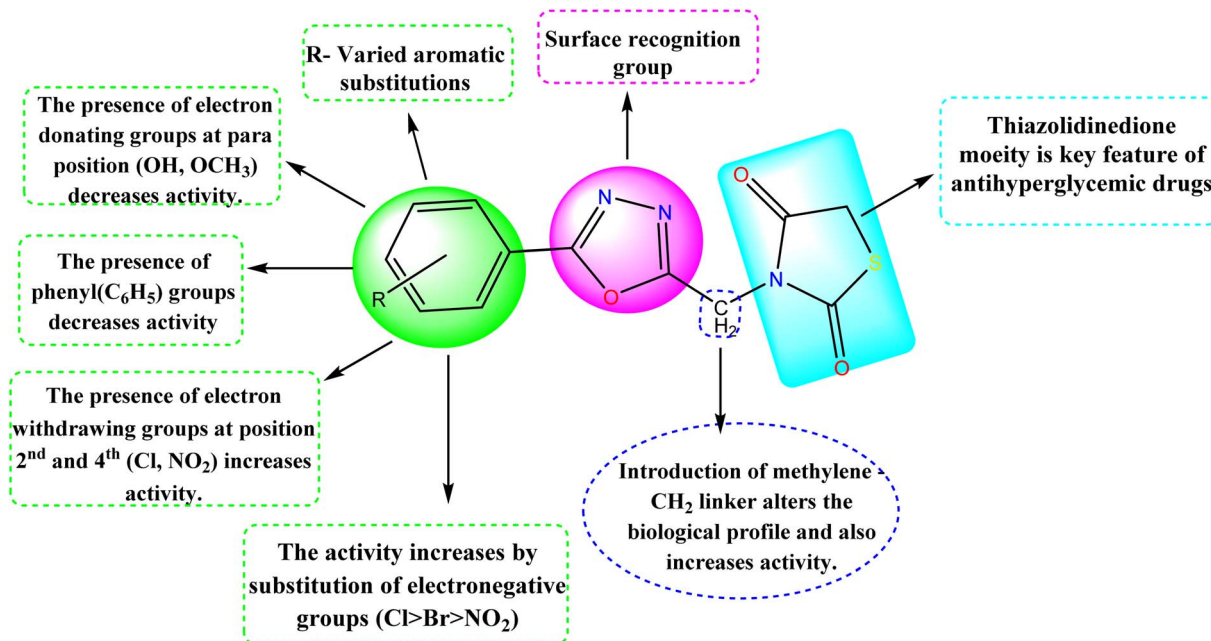**Fig. 5** *In vivo* testing for antihyperglycemic effects in *Drosophila melanogaster* ((a) male; (b) female).

The presence of electron donating groups at para position (OH, OCH₃) decreases activity.

R- Varied aromatic substitutions

Surface recognition group

Thiazolidinedione moeity is key feature of antihyperglycemic drugs

The presence of phenyl(C₆H₅) groups decreases activity

The presence of electron withdrawing groups at position 2ⁿᵈ and 4ᵗʰ (Cl, NO₂) increases activity.

The activity increases by substitution of electronegative groups (Cl>Br>NO₂)

Introduction of methylene CH₂ linker alters the biological profile and also increases activity.

Fig. 6 Structure–activity relationship (SAR) of the compounds (**5a–5j**).
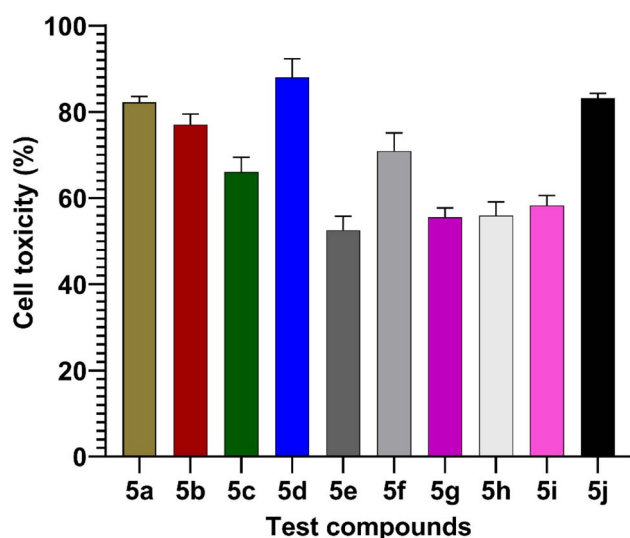
Fig. 7 Values are mean ± SD from triplicate determined ($n = 3$). The percentage cell toxicity of different test compounds (**5a–5j**) at a concentration of 100 μmol.

The compounds **5d** (87%) and **5j** (83%) showed higher cell toxicity when compared to other tested compounds (Fig. 7).

Conclusion

This research represents the synthesis of novel series of 3-((5-phenyl-1,3,4-oxadiazol-2-yl)methyl)thiazolidine-2,5-dione derivatives. All the synthesized compounds were confirmed by spectroscopic methods and evaluated for *in vitro* anti-hyperglycemic activity by α-amylase and α-glucosidase inhibition assay. *In vivo*, *Drosophila melanogaster* fly model was used to test the efficacy of

these compounds and was raised on a diet containing even concentrations of either acarbose or compounds with most *in vitro* activity, *i.e.*, **5a**, **5b**, and **5j** from the results. There was a significant difference between standard acarbose and the compounds **5a**, **5b**, and **5j** in terms of antihyperglycemic activity. Therefore, clinical research has become increasingly concerned with developing compounds with antihyperglycemic activity. Considering this, it was found that compounds **5a**, **5b**, and **5j** had both these properties. The findings indicated that these compounds might provide a rational approach to the development of novel and potent diabetes genetic enzyme inhibitors. However, the study requires further preclinical trials and these compounds can be used as very good candidates for the effective therapeutic management of diabetes mellitus.

Author contributions

RBC did the conception of the work, design of the work, experimental work, and the interpretation of data and drafting of the manuscript. MGS and JGP contributed to the design of work, experimental work done, and results in analysis. AP, VP, and SRSB helped in carrying out the design work, and MGS, SDN, and RBC reviewed the manuscript. All authors read and approved the final manuscript.

Conflicts of interest

There are no competing financial interests or personal relationships influencing the findings of this paper.

Acknowledgements

References

1 M. Sherafati, R. Mirzazadeh and E. Barzegari, *Bioorg. Chem.*, 2021, **109**, 104703.

2 S. Hati, S. M. Madurkar, C. Bathula, C. Thulluri, R. Agarwal, F. A. Siddiqui, P. Dangi, U. Adepally, A. Singh, S. Singh and S. Sen, *Eur. J. Med. Chem.*, 2015, **100**, 188–196.

3 N. C. Jadhav, A. R. Pahelkar, N. V. Desai and V. N. Telvekar, *Med. Chem. Res.*, 2017, 2675–2691.

4 T. I. Solikhah, B. Setiawan and D. R. Ismukada, *Syst. Rev. Pharm.*, 2020, **11**, 774–778.

5 S. Chiba, *Biosci., Biotechnol., Biochem.*, 1997, **61**(8), 1233–1239.

6 R. Mehmood, A. Sadiq, R. I. Alsantali, E. U. Mughal, M. A. Alsharif, N. Naeem, A. Javid, M. M. Al-rooqi, G. Chaudhry and S. A. Ahmed, *ACS Omega*, 2022, **7**(4), 3775–3795.

7 A. Toumi, S. Boudriga, K. Hamden, M. Sobeh, M. Askri, M. Knorr and C. Strohmann, *Bioorg. Chem.*, 2020, 104507.

8 M. Asgher, M. J. Asad, S. U. Rahman and R. L. Legge, *J. Food Eng.*, 2007, **79**(3), 950–955.

9 M. D. P. T. Gunawan-puteri, E. Kato and J. Kawabata, *J. Sci. Food Agric.*, 2012, **92**(3), 606–609.

10 N. Jong-anurakkun, M. R. Bhandari and J. Kawabata, *Food Chem.*, 2007, **103**(4), 1319–1323.

11 U. Salar, K. M. Khan, S. Chigurupati and M. Taha, *Sci. Rep.*, 2017, 1–17.

12 H. A. Abuelizz, N. A. Iwana, R. Ahmad, E. H. Anouar, M. Marzouk and R. Al-Salahi, *BMC Chem.*, 2019, **13**(1), 1–4.

13 P. Kumar, M. Duhan, J. Sindhu, K. Kadyan, S. Saini and N. Panihar, *J. Heterocycl. Chem.*, 2020, **7**(4), 1573–1587.

14 M. A. Huneif, D. Batti, K. S. Alshaibari, M. Z. Dammaj, M. H. Mahnashi, S. Ullah, M. Aamir, S. Ahmad, U. Rashid and A. Sadiq, *Biomed. Pharmacother.*, 2022, **150**, 113038.

15 O. Zvarec, S. W. Polyak, W. Tieu, K. Kuan, H. Dai, D. Sejer, R. Morona, L. Zhang, G. W. Booker and A. D. Abell, *Bioorg. Med. Chem. Lett.*, 2012, **22**, 2720–2722.

16 E. F. Cosma, M. Laichici, G. F. Cosma and D. Vlascici, *J. Serb. Chem. Soc.*, 2006, **71**, 1031–1038.

17 S. Abdel, G. Abdel, T. El, S. Ali, K. Mohamed, E. Mahdy, S. Mohamed and A. Karim, *Eur. J. Chem.*, 2011, **2**, 25–36.

18 Y. Haribabu, K. Srinivasulu, C. S. Reddy and C. D. Reddy, *Arkivoc*, 2006, **15**, 95–103.

19 T. Lichtor, A. Spagnolo, R. P. Glick and D. L. Feinstein, *PPAR Res.*, 2008, 547470.

20 M. J. Nanjan, M. Mohammed, B. R. P. Kumar and M. J. N. Chandrasekar, *Bioorg. Chem.*, 2018, **77**, 548–567.

21 Y. Zhao, Q. Zheng, K. Dakin, K. Xu, M. L. Martinez and W. H. Li, *J. Am. Chem. Soc.*, 2004, **126**(14), 4653–4663.

22 J. R. Hwu, S. Y. Lin, S. C. Tsay, E. De Clercq, P. Leyssen and J. Neyts, *J. Med. Chem.*, 2011, **54**(7), 2114–2126.

23 I. Khan, A. Ibrar and N. Abbas, *Arch. Pharm.*, 2014, **347**(1), 1–20.

24 U. Jayaram, M. A. Azam, A. D. Wadhwani, S. K. Verma, K. Rathinasamy and S. Mahanty, *Jordan J. Pharm. Sci.*, 2020, **13**, 337–361.

25 S. Bala, S. Kamboj, A. Kajal, V. Saini and D. N. Prasad, *Biomed. Chem. Res.*, 2014.

26 T. Qidwai, *In Silico Pharmacology*, 2017, **5**, 1–13.

27 F. Peter Guengerich, *Drug Metab. Pharmacokinet.*, 2011, **26**, 3–14.

28 R. Alnajjar, A. Mostafa, A. Kandeil and A. A. Al-karmalawy, *Heliyon*, 2020, **6**, e05641.

29 F. Cheng, W. Li, Y. Zhou, J. Shen, Z. Wu, G. Liu, P. W. Lee and Y. Tang, *J. Chem. Inf. Model.*, 2012, **52**, 3099–3105.

30 J. Li, R. Abel, K. Zhu, Y. Cao, S. Zhao and R. A. Friesner, *Proteins: Struct., Funct., Bioinf.*, 2011, **79**(10), 2794–2812.

31 M. Gowdru, S. Natasha, N. Aggarwal, B. Felicity, D. Gatpoh, M. Kumar, K. Byadarahalli, R. Pujar, G. Veeranna, S. Dixit, S. P. Mandal, P. Kumar, B. Ravanappa, P. Khanal and R. B. Chandrashekarappa, *J. Mol. Recognit.*, 2022, 2959.

32 R. S. Gani, A. K. Kudva, K. Timanagouda, S. Begum, H. Mujawar, S. D. Joshi and S. Varija, *Bioorg. Chem.*, 2021, **114**, 105046.

33 M. Danihelova, M. Veverka, E. Sturdík and S. Jantova, *Interdiscip. Toxicol.*, 2013, **6**(4), 209–216.

34 G. Oboh and O. Babatunde, *Biomed. J.*, 2019, **42**, 317–327.

35 S. A. Ross, E. A. Gulve and M. Wang, *Chem. Rev.*, 2004, **104**(3), 1255–12827.

36 O. H. Oyeniran, A. O. Ademiluyi and G. J. Oboh, *Food Biochem.*, 2021, **45**(3), 13318.